NOTICE: this is the author's version of a work that was accepted for publication in International Journal of Machine Tools and Manufacture. Changes resulting from the publishing process, such as peer review, editing, corrections, structural formatting, and other quality control mechanisms may not be reflected in this document. Changes may have been made to this work since it was submitted for publication. A definitive version was subsequently published in International Journal of Machine Tools and Manufacture, Volume 48, Issue 15, December 2008. doi:10.1016/j.ijmachtools.2008.07.008

Machining of metal matrix composites: effect of ceramic particles on residual stress, surface roughness and chip formation

A. Pramanik, L. C. Zhang* and J. A. Arsecularatne

School of Aerospace, Mechanical and Mechatronic Engineering, The University of Sydney, NSW 2006, Australia

Abstract

Machining forces, chip formation, surface integrity and shear and friction angles are important factors to understand the machinability of metal matrix composites (MMCs). However, because of the complexity of the reinforcement mechanisms of the ceramic particles, a fair assessment of the machinability of MMCs is still a difficult issue. This paper investigates experimentally the effects of reinforcement particles on the machining of MMCs. The major findings are: (1) The surface residual stresses on the machined MMC are compressive; (2) The surface roughness is controlled by feed; (3) Particle pull-out influences the roughness when feed is low; (4) Particles facilitate chip breaking and affect the generation of residual stresses; and (5) The shear and friction angles depend significantly on feed but are almost independent of speed. These results reveal the roles of the reinforcement particles on the machinability of MMCs and provide a useful guide for a better control of their machining processes.

Keywords: Metal matrix composite, residual stress, surface roughness, chip formation.

* Corresponding author. Tel.: +61 2 93512835; fax: +61 2 93517060
Email address: zhang@aeromech.usyd.edu.au (L. C. Zhang)

Nomenclature

A_c	Cross sectional area of cut
B, C	Constants in Eq. 7
R_a	Arithmetic mean value of surface roughness
R_{max}	Maximum peak to valley height of surface roughness within the sampling length
F_{cc}	Chip formation force in cutting
F_{ct}	Chip formation force in thrust
f	Feed
r_c	Chip thickness ratio (defined as cut-thickness divided by chip thickness)
r_ε	Tool nose radius
β	Mean friction angle
γ	Tool rake angle.
ϕ	Shear angle
τ_s	Experimental shear strength

1. Introduction

Aluminium alloys have a high machinability index and have been enormously used in aerospace and automobile industries due to their superior properties such as higher strength to weight ratio, excellent low temperature performance, exceptional corrosion resistance, chemical inertness to commonly used cutting tools, etc [1]. However, the main weaknesses of aluminium alloys are their poor high temperature performance and wear resistance. To overcome these problems, aluminium alloys reinforced by ceramic particles, known as metal matrix composites (MMCs), have been developed [2-9]. Nevertheless, the incorporation of the hard particles makes the machining of MMCs difficult [10, 11], and diamond tools are often necessary [8, 12-14].

There have been some investigations on the machining of MMCs, dealing with tool wear [13-15], surface/subsurface quality [14, 15] and chip formation [15-17], but systematic studies on the effect of machining parameters on forces, surface integrity and chip formation in relation to the reinforcement are not available.

The objective of this paper is to gain a deeper understanding of the effects of reinforced particles on forces, surface roughness, residual stress, chip shape and, shear and friction angles with varied machining parameters when cutting MMC specimen.

2. Experiment

The experiments were made on a CNC Turning Centre, Mori-Seiki MT 2000α1s2, using a bar turning process under dry conditions.

The specimens (denoted as (2) in Fig. 1) were made of non-reinforced 6061 aluminium alloy and an MMC made of same alloy reinforced with 20 vol% SiC particles (particle size = 6-18 μm) in 6061 aluminium matrix (designated as F3S.20S in Alcan's literature). The tools (denoted as (3) in Fig. 1) were polycrystalline diamond tipped TPMN 160304 inserts (CTH025 grade from Element-6) on tool holder CTGPR2525-M16 (denoted as (4) in Fig. 1). Their nose radius, rake angle and approach angle were 0.4 mm, 5º and 90º, respectively. The cutting edge radius (without edge hone) was measured to be 5.42 μm.

The cutting conditions were: depth of cut = 1.0 mm; feed = 0.025, 0.05, 0.1, 0.2 and 0.4 mm/rev; and cutting speed = 100, 200, 400, 600 and 800 m/min. The ranges of cutting conditions selected were based on the recommendations in the literature and from the tool manufacturer. During experiments, only one of the above parameters was varied while others were held constant to observe the effects of variation of an individual input parameter on the output parameters.

A Kistler 9121 three-axis piezo-electric dynamometer (denoted as (5) in Fig. 1) with a PC based data acquisition system was used to measure the cutting forces.

For each test, cutting was performed for over 10 seconds. Replication tests under selected conditions were made to verify repeatability. The chip thickness was measured using a micrometer. Surface roughness was measured by Mitutyo Surftest 402. An optical microscope (Wild Heerbrugg) was used to observe chips and machined surfaces. Residual stresses along longitudinal and transverse directions of the machined surfaces were measured on an X-ray diffraction machine, Rigaku MSF-3M.

3. Results and discussion

3.1 Forces

The measured cutting and thrust forces at different feeds are presented in Fig. 2. It can be seen that cutting force for the non-reinforced aluminium alloy is slightly larger than that for the MMC (Fig. 2 (a)). For the two materials, the experimental cutting forces increase more or less linearly with the increase in feed and the rate of increase is almost similar. Thrust forces increase at a lower rate than the cutting forces (Fig. 2 (b)). At lower feeds, thrust force for non-reinforced alloy is higher than that for MMC but above certain feed, the opposite trend is noticed. At this stage, similar rate of increase of forces is noted for the two materials. Thrust forces are higher than cutting forces at lower feeds (below 0.1 mm/rev) but the opposite is observed at higher feeds.

Figs. 3(a) & (b) present the variation of cutting and thrust forces at different cutting speeds for the MMC and aluminium alloy. In case of MMC, speed does not influence the two forces significantly. For non-reinforced alloy, both forces are lower than those of MMC at low cutting speed but with the increase of speed the forces increase and at certain stage they are higher than those of MMC. With further increase of speed, the forces start to decrease (due to thermal softening) and at certain stage they again become lower than those of MMC. The cutting forces are higher than thrust forces for both materials at all cutting speeds considered in this investigation.

In a previous paper [4], the authors reported a mechanics model for predicting forces when cutting MMCs where the force generation was considered to be due to three factors (a) chip

formation, (b) particle fracture/debonding and (c) ploughing. Cutting/thrust forces due to chip formation, particle fracture/debonding and ploughing were calculated for the MMC in the present work. The percentages of these forces in cutting and thrust directions are presented against feed and speed in Figs. 4 & 5, respectively. It is found that percentages of chip formation force is much higher (80-97%) compared to particle fracture/debonding (1.5-20%) and ploughing (0.25-2%) forces. The percentages of particle fracture/debonding and ploughing forces in cutting direction decrease and chip formation force increases with the increase of feed (Fig. 4(a)). The percentages of particle fracture/debonding and plougning forces are lower and higher, respectively, in the thrust direction compared to those in cutting direction (Fig. 4(b)). No significant change of percentages of forces is noted with the variation of feed in the thrust direction. With the variation of speed, the percentages of different forces in cutting and thrust directions do not seem to vary (Figs. 5(a) & (b)). The percentages of particle fracture/debonding forces in the thrust direction are considerably low compared to those in the cutting direction.

The chip formation forces during turning depend on the strength of the material, cutting conditions and tool geometry. Speed and feed influence the strength of the workpiece material in the deformation zones through temperature, strain and strain rate [4, 18]. The strength of the non-reinforced aluminium alloy is nearly insensitive to strain rate at low strain and strain rate [19-21]. But at higher strains (more than 1) and strain rates (10^3 s^{-1} or higher), i.e., those experienced during turning [22-24], the strength is considerably dependent on strain rate and it increases with the increase of strain rate [25-27]. In the present work, for simplicity, the effects of strain, strain rate and temperature on shear strength are not considered explicitly. However, it was found that, the measured F_{cc}[1] and F_{ct} (chip formation forces in cutting and thrust directions, respectively), and ϕ (shear angle) depend on the cutting conditions. Hence, the experimental shear strength values, τ_s,

[1] Chip formation forces were calculated by deducting ploughing and particle fracture/debonding forces from total machining forces.

for both the aluminium alloy and MMC at different machining conditions were determined using Eq. (1) following the procedure described in [4, 22].

$$\tau_S = \frac{\left[\left(F_{CC}\cos\phi\right) - \left(F_{Ct}\sin\phi\right)\right]\sin\phi}{A_C} \qquad (1)$$

The shear strength values of MMC and non-reinforced alloy for different machining conditions are presented in Fig. 6. It can be seen that the strength of MMC is significantly lower than that of non-reinforced alloy for all the machining conditions considered. At low feeds, the strength of MMC and non-reinforced alloy decreases with the increase of feed (Fig. 6(a)). However, at higher feeds, τ_s does not vary with feed significantly. Speed does not influence the strength of MMC significantly (Fig. 6(b)). At lower range of speed, strength of non-reinforced alloy increases with the increase of speed but after certain speed it decreases with further increase of speed.

At low feed (cut thickness), the area of cut is small and the entire cut area may have been work hardened by previous tool pass. This will result in a higher τ_s value at lower feed than that at higher feed. Increased percentage of particle fracture/debonding forces (Fig. 4) indicates higher tool-particle interaction at low feed for MMC which may be another reason for increased strength at low feed [11]. Consequently, higher strength of workpiece materials is noted at low feed. However, with increase of feed, work hardening decreases and temperature increases canceling out the net variation of strength of MMC and non-reinforced alloy.

Note that the strength of the two workpiece materials decrease with the increase of feed (at feeds below 0.2 mm/rev). However, the cutting forces increase due to increase in area of cut (Figs. 2(a) & (b)).

For the non-reinforced alloy, at low cutting speeds, temperature generation is considerably low [6]; hence the increase of strength and forces with cutting speed is likely to be due to the influence of increase of strain rate. With further increase of cutting speed, machining temperature increases, consequently thermal softening of workpiece material occurs. However, the increase in strain rate

will increase the strength of the material [19]. It seems that after certain speed, thermal softening becomes dominant over the strain hardening resulting in decrease in strength and forces [1, 19].

Similar to the non-reinforced alloy, work hardening of MMC increases with the increase of strain rate and decrease with the increase of temperature [25]. Researches found that composite material may display considerably greater strain rate sensitivity (i.e. increase in forces with cutting speed) than that of non-reinforced material [28, 29]. But the lower strength (Figs. 6(a) & (b)) of MMC during machining may be a result of cracks generated due to presence of particles in the shear planes and tool-chip interface [10, 30, 31].

To study the influence of tool-particle interactions on force generation, force signals from dynamometer were investigated. Force signals at different cutting conditions for the MMC and non-reinforced alloy during cutting are presented in Fig. 7. No significant influence of these interactions on the force signals is noted as the signals are similar for the MMC and non-reinforced materials. This may be due to smaller inter particle distance in MMC. It is estimated that for MMC with 20 volume percentage (uniformly distributed spherical particles) of reinforcement (size 12 μm) the inter particle distance is ~ 4.5 μm. At minimum cutting speed 100 m/min, cutting tool will travel this distance in only 0.0027s and it seems that the data acquisition system used is not fast enough to detect individual tool-particle interactions. In addition, at depth of cut 1 mm, since the length of the active cutting edge is over 1 mm and particles are more or less uniformly distributed in the MMC, continuous tool-particle interactions will occur along the cutting edge. Hence, the effect of individual tool-particle interaction on the force signal is not likely to be distinguishable.

3.2 Surface roughness

A surface is difficult to achieve because of fracture and pull-out of particles during machining of an MMC [10, 32]. Hence, the effect of machining parameters on machined MMC surface may be different to that on a non-reinforced material surface. The theoretical roughness of a turned surface (due to feed marks) can be calculated by using the following equations [12, 33]:

$$R_a \approx \frac{0.032 f^2}{r_\varepsilon} \quad (2)$$

$$R_{\max} \approx \frac{f^2}{8 r_\varepsilon} \quad (3)$$

where R_a is the arithmetic mean value of surface roughness which does not indicate actual profile of surface but gives an idea of average surface geometry, R_{max} is the maximum peak to valley height within the sampling length, f is feed and r_ε is tool nose radius. Theoretical R_a and R_{max} values obtained by Eqs. (2) & (3) are also compared with the experimentally obtained surface roughness in the following sections.

3.2.1 Effect of feed

The profile of surface roughness can be considered as successive movements of the tool profile at intervals of feeds. Figs. 8(a) & (b) show the variation of measured surface finish (R_a and R_{max}) with feeds. As expected, surface roughness is low at low feed and it increases with increase of feed for the both reinforced and non-reinforced materials. At low feeds, roughness for the MMC is higher than that for non-reinforced alloy but above feed 0.3 mm/rev, the reverse trend is observed. The theoretical roughness values are lower than experimental values for both materials, though the deviation of experimental roughness from theoretical one is much smaller at low feed.

The machined MMC surfaces in Fig. 9 show that the feed marks are not noticeable at lower feeds and surface texture is very irregular likely due to the presence of particles (Fig. 9). On the other hand feed marks are very clear on the non-reinforced alloy surface at all feeds and burr formation is clearly visible at higher feed (0.4 mm/rev) (Fig. 10).

3.2.2 Effect of speed

Fig. 11 depicts the effect of reinforcement particles on surface roughness at different speeds. It is noted that the non-reinforced alloy show better roughness compared to MMC at all cutting speeds investigated. In general the surface roughness slightly decreases with the increase in cutting speed for both materials. This may be due to lower side flow of material at higher cutting speed. Similar

to the influence of feed discussed above, the theoretical roughness values are much lower than experimental roughness values.

From Figs. 12 & 13, it is clear that unlike machined surface of non-reinforced alloy, no feed marks were noted on the MMC surface. Additionally no noticeable influence of speed on the machined MMC and non-reinforced alloy surfaces is noted for the range of speeds considered.

For the MMC, absence of feed marks at low feed may be due to pull out and fracture of particles from the machined surface and indentation by particles. These are considered to be dominating factors that influence the texture of the newly generated surface [10, 14, 17, 32, 34]. For a given length of cut, at low feed, the distance between two successive tool paths is less and hence a higher number of tool-particle interactions will occur than at higher feed. Relatively high particle fracture/debonding force at lower feed (discussed in Sec. 3.1) also indicates higher tool-particle interactions. These will cause higher surface damage at low feed. In the case of non-reinforced alloy no such damage is expected at low feed which account for its better surface finish. At higher feed, the crest (due to side flow of material) on feed mark ridges of surface likely to exist due to its high ductility (Fig. 10, at feed 0.4 mm/rev). In the case of MMC, those may not exist due to lower ductility of MMC and its tendency to fracture (Fig. 9). These may cause higher roughness of the non-reinforced alloy surface compared to that of MMC.

This can be further investigated using the profiles of machined MMC and non-reinforced alloy surfaces which, at various feeds, are given in Figs. 14 & 15, respectively. It can be seen that MMC surface profile is very irregular at low feeds but with the increase of feed, the feed marks are clearly recognized in the surface profile. On the other hand, for the non-reinforced alloy, very smooth surface profiles are noted at low feeds. However, surface profile is dominated by feed marks at higher feeds. For the MMC, it is noted that at low feeds (0.025-0.1 mm/rev) the magnitude of R_{max} varies from 7-12 μm which is in the range of particle size (6-18 μm). It appears that, for the range of feeds considered in this study, the surface roughness of MMC is influenced by particle size at low feeds.

3.3 Residual stress

An important parameter of a machined component's surface integrity is the residual stress distribution which determines the fatigue life, etc. Residual stresses are related to the incompatibility between a surface layer and the bulk material which is generated by any mechanism that generates a variation in the geometry of the surface layer [35]. These stresses depend on workpiece material and machining parameters such as the cutting speed and feed. Only few studies on turning induced residual stress of monolithic (non-reinforced) materials have been reported to date [35-39]. These suggest that both the mechanical and thermal effects are responsible for the generation of residual stresses on the machined surface. Considering that the machining and deformation mechanisms of an MMC are more complicated and different to those of a monolithic (non-reinforced) material, the mechanisms of residual stress generation are likely to be more complex for the former. As a result, the effects of machining parameters on surface residual stress may not be the similar when the reinforced particles are present. The effect of reinforcement particles on the residual stress generation on the machined surface with the variation of machining parameters is compared and discussed in the following sections.

3.3.1 Effect of feed

Fig. 16(a) shows that the longitudinal (parallel to the axis of the machined bar) residual stress on the machined non-reinforced alloy surface is tensile for the whole range of feeds considered but it is compressive for the MMC. The magnitude of the tensile residual stress (10-140 MPa) is much larger than the compressive one (0-16 MPa). The residual stress of the non-reinforced alloy is low at low feed but with the increase of feed, it increases at a very high rate. After a certain feed, this rate is decreased and very little further increase of residual stress is noted. For the MMC, the compressive residual stress decreases and moves towards the neutral at a low rate with the increase of feed. The transverse (perpendicular to the axis of the machined bar) residual stress (Fig. 16(b))

for the non-reinforced alloy shows a similar trend to its longitudinal one. The transverse residual stress for the MMC is nearly neutral and does not vary significantly with feed (Fig. 16(b)).

3.3.2 Effect of speed

Fig. 17(a) shows that the residual stress (longitudinal) is tensile (10-100 MPa) in machined surface of the non-reinforced alloy and compressive (3-12 MPa) in that of the MMC for the considered range of speeds. Longitudinal residual stress for non-reinforced alloy is low at lower cutting speed and it increases at a high rate with the increase of speed and then reaches a constant value. The influence of speed on longitudinal residual stress on the MMC surface is negligible. The transverse residual stress in the non-reinforced alloy is also tensile and increases at almost constant rate with the increase of speed (Fig. 17(b)). Similar to longitudinal residual stress, the transverse residual stress in machined MMC surface does not vary significantly with the variation of speed for the range considered.

From the above discussion it is clear that the residual stress in the machined non-reinforced alloy surface is tensile but it is compressive in the MMC for all the conditions considered. Capello [35] divided the mechanisms of residual stress generation into three categories: mechanical (plastic deformation), thermal (thermal plastic flow) and physical (specific volume variation). Tensile residual stresses are caused by thermal effects and compressive stresses by mechanical effects related to the machining operation. The relatively small compressive stress measured on the MMC surface indicates marginally higher influence of mechanical factor compared to thermal factor. On the other hand, thermal effects play prominent role over mechanical effects in the residual stress generation when reinforced particles are absent. The influence of thermal factor for non-reinforced alloy increases with increase in feed/speed.

For the MMC, based on the machining and indentation investigations [10, 11], it appears that three factors are mainly responsible for excessive mechanical deformation on the machined surface that take over the thermal effects. These factors are (a) restriction of matrix flow due to presence of

particles (b) indentation of particles on the machined surface and (c) high compression of matrix in between particles and tool. At low feed, these factors become very prominent. Increased percentage of particle fracture/debonding forces (Fig. 4) indicates higher tool-particle interaction at low feed. However, with the increase of feed, indentation effects of particles as well as tool particle interaction decreases for the same length of machined workpiece. Additionally, effects of temperature increase with the increase of feed. Thus high compressive residual stress values at low feed and lower stress values at higher feed can be expected.

The influence of temperature is comparatively small at low cutting speed but with the increase of speed its influence increases [32]. The influence of mechanical factors also increases due to increase in strain rate. With varying speed, it appears that the mechanical and thermal effects balance out resulting in a negligible compressive residual stress on the machined MMC surface.

3.4 Chip shape

Compared to the non-reinforced alloy, chips of different shapes were noted during machining of the MMC. The types of chips formed are related to the material properties and cutting parameters such as speed, feed, etc. [40]. Effect of reinforcement particles on chip shape under different machining parameters is discussed in the following sections.

For the MMC, chip shapes vary over the considered range of feeds as shown in Fig. 18. At feed 0.025 mm/rev, chips were very short and irregular in shape. With the increase of feed long chips were formed. At feeds 0.05 and 0.1 mm/rev, long spiral and straight chips, respectively, were observed. With further increase of feed (0.2 and 0.4 mm/rev), all chips became short and of C-shape. Though at medium feeds chips were very long, it did not entangle with the tool or workpiece and it was easily breakable. For the non-reinforced alloy, it is found that in general, the chip shape did not change significantly with the increase of feed (Fig. 19). At all feeds, chips were long, little twisted and, had a tendency to entangle with the tool and workpiece which damaged the newly generated surface.

With the variation of cutting speed, very long and brittle chips were formed for MMC (Fig. 20). At lower speed (100 and 200 m/min) all the chips were of spiral shape but at higher speeds chips became straight (400 and 600 m/min). With further increase of speed (800 m/min), some tightly curled chips were formed together with long straight chips. For the non-reinforced alloy, at all cutting speeds chips were long and large spirals which entangled with the workpiece and tool (Fig. 19).

Continuous chips are forced to curl during formation due to unequal strain occurring across the plastic zone [41]. The curl depends on ductility/brittleness of the chips. Chips of brittle materials have little or no tendency to curl but those of ductile materials may form long spiral chips. Shapes of chips are influenced by the uniformity of deformation and shear localization [42]. During deformation of the MMC, stress concentrations and local deformations are experienced due to presence of reinforced particles [10, 11]. As MMC experiences high strain while passing through the primary and secondary shear zones, some particles are debonded initiating cracks and work hardening the matrix material [10, 30, 31, 43]. This makes chips brittle and easy to fracture, resulting in the formation of short chips. At lower feed, deformation of chip is more homogeneous across its thickness which may lead to formation of longer chips. But it seems that if feed is very low, chips become very thin which may break due to failure of highly strained particle-matrix interface. On the other hand, at higher feed, considerable non-homogeneous deformation occurs due to higher cut/chip thickness which contributes to generation of shorter chips. Similarly at low cutting speed, strain rate effect is prominent which may cause inhomogeneous deformation resulting in the formation of spiral chips but with the increase of speed thermal effects may reduce the inhomogeneous deformation of chips and increase the ductility of matrix [32] which produces straight chips.

All the chips formed during machining of the non-reinforced alloy were long and ductile because of its high ductility and deformation without formation of cracks due to absence of particles.

A harder material generally exhibits better chip disposability and shorter chips with brittle fracture in the chips as well as on the machined surface. On the other hand, ductile material produces very long chips with poor disposability. Long chips damage the newly generated surface. Ductile cutting with short chips are normally desired to obtain an undamaged surface [44]. It seems that hard reinforcement particles in the MMC introduce disposability to highly ductile matrix material.

3.5 Shear and friction angles

Shear and friction angles are associated with machining forces, efficiency of metal removal process, surface roughness and tool wear. Shear angle is calculated from chip thickness ratio which is a measure of plastic deformation in metal cutting. Generally a ductile material will have a low shear angle and a brittle material will have a large shear angle [17]. The shear angle ϕ is calculated by using the relation:

$$\phi = \tan^{-1}\left(\frac{r_c \cos\gamma}{1 - r_c \sin\gamma}\right) \qquad (4)$$

where r_c is chip thickness ratio (defined as cut-thickness divided by chip thickness) and γ is the tool rake angle.

Friction angle controls the temperature generation at the tool chip interface and hence crater wear. This parameter can be derived from the associated cutting and thrust forces using the equation:

$$\beta = \tan^{-1}\left(\frac{F_{cc} + F_{ct}\tan\gamma}{F_{cc} - F_{ct}\tan\gamma}\right) \qquad (5)$$

where β is the mean friction angle, F_{cc} is the chip formation force in the cutting direction, F_{ct} is that in the thrust direction and γ is the tool rake angle. A higher friction angle will result in a higher temperature generation at tool chip-interface and hence high tool wear. Applicability of Eqs. (4) and (5) for MMC machining were considered in [4, 22, 45].

Fig. 21(a) shows the effect of reinforced particles on the shear angle with the variation of feed. The shear angle increases with the increase of feed for both workpiece materials. Initially its rate of increase is very high and shear angle for the MMC is higher than that for the non-reinforced alloy. After certain feed it becomes higher for the non-reinforced alloy. Then the variation of shear angle with feed reduces for both materials. According to Eq. (4) higher shear angle means lower chip thickness or higher chip thickness ratio (r_c). During machining, the chip undergoes a complete deformation across its thickness in the primary shear zone but in the secondary shear zone, deformation is restricted to the tool-chip interface region. Therefore, with the increase of cut thickness the thickness of secondary deformation of chips reduces compared to total chip thickness. This causes inhomogeneous deformation of chips and generation of well broken C-shaped chips for the MMC (Fig. 18).

The effect of reinforced particles on friction angle with the variation of feed is presented in Fig. 21(b). The friction angle curves are of hyperbolic shape for the MMC and non-reinforced alloy. Initially the friction angle for the non-reinforced alloy is little higher than that for the MMC and they start to decrease at high rate with the increase of feed. Above certain feed the friction angle for the non-reinforced alloy becomes lower than that for the MMC. With further increase of feed this angle continues to decrease at a reduced rate for both materials.

The variation of shear angle with speed due to presence and absence of particles is depicted in Fig. 22(a). Shear angles for the non-reinforced alloy are higher than those for the MMC over the range of speeds considered in this investigation. For the non-reinforced alloy, shear angle initially decreases with the increase of cutting speed then it starts to increase at a small rate with further increase of speed. This reflects initial increase of force with speed and then decrease after certain speed (Section 3.1). The shear angle for the MMC continuously increases with the increase of feed at a low rate.

Fig. 22(b) shows the effect of particles on friction angle with the variation of cutting speed. Unlike the shear angles, friction angles for the MMC are higher than those for the non-reinforced

alloy for the whole range of speeds considered. At low speed, comparatively low friction angle is noted for the non-reinforced alloy but it increases rapidly with the increase of speed and reaches a constant value with further increase of speed. A small increase of friction angle for the MMC is noted with the increase of speed.

3.6 Relation between shear and friction angles

As noted earlier, the shear angle ϕ is associated with geometry of chip formation and hence cutting forces, etc. The theoretical relations obtained for ϕ by Merchant [46] and Lee and Shaffer [47] are:

$$\phi = \begin{cases} \frac{\pi}{4} - \frac{1}{2}(\beta - \gamma) & \textit{Merchant} \\ \frac{\pi}{4} - (\beta - \gamma) & \textit{Lee and Shaffer} \end{cases} \qquad (6)$$

where β and γ are friction and rake angles, respectively.

However, the experimental results obtained by investigators such as Kobayashi and Thomson [48] and Pugh [49] for a wide range of work materials (monolithic) and cutting conditions show that the following relation is more appropriate for ϕ.

$$\phi = B - C(\beta - \gamma) \qquad (7)$$

where *B* and *C* are constants which depend on the work material.

Figs. 23(a) and (b) show the experimental values of ϕ plotted against $(\beta - \gamma)$ for the MMC and non-reinforced alloy. For MMC, data from all the machining conditions of this investigation as well as from investigation in Ref. [4] was used. The linear regression lines for the data are also shown in the figures. It can be seen that the experimental results fall close to the lines represented by the Eqs. (8) and (9) for the MMC and non-reinforced alloy, respectively.

$$\phi = \frac{\pi}{5} - \frac{1}{2}(\beta - \gamma) \qquad \textit{for MMC} \qquad (8)$$

$$\phi = \frac{\pi}{4} - \frac{1}{2}(\beta - \gamma) \qquad \textit{for non-reinforced alloy} \qquad (9)$$

It can be seen that, similar to the case of cutting monolithic materials discussed above, there also exists a linear relationship between ϕ and $(\beta - \gamma)$ even for the MMC. In the case of the non-reinforced alloy, the relationship is similar to Merchant's equation (Eq. (6)). The notable difference is that the value of *B* (Eq. (7)) for the MMC is not identical to that for the matrix material (Eqs. (8) & (9)).

4. Conclusions

This study has systematically investigated the machinability of MMCs and the effect of reinforcement particles on machining forces, chip formation, surface integrity and shear and friction angles. The following conclusions can be drawn:

(i) For turning of the MMC and non-reinforced alloy, cutting forces of similar magnitude were noted and they increased with the increase of feed. However, speed did not influence forces significantly for the MMC. On the other hand, forces for the non-reinforced alloy were initially lower than those for the MMC and increased with speed. After certain speed they started to decrease and were lower than the forces for MMC. This complex variation of forces for MMC and its alloy were due to the following factors: (a) different work hardening properties of these materials, (b) fracture at the shear plane and tool-chip interface for MMC, (c) different thermal softening behavior of these materials, (d) tool-particle interactions for MMC, and (e) different effects of strain and strain rate on the responses of these materials.

(ii) At low feeds, the surface roughness of the MMC was controlled by particle fracture or pull out but at higher feeds, it was controlled by the feed. On the other hand, surface roughness of the non-reinforced alloy was mainly controlled by the feed.

(iii) The effect of speed and feed on residual stress for the machined non-reinforced alloy surface was different to that for the MMC. Both longitudinal and transverse residual stresses on the matrix surface were tensile and increased with the increase of speed and feed. On the other hand, presence of reinforcement particles induced compressive residual stresses on the machined MMC surface due to their interaction with the cutting tool. Increase of feed reduced the longitudinal compressive residual stress but had negligible influence on the transverse stress. The influence of speed on the residual stress of the MMC was not significant.

(iv) Chip breakability was found to improve due to the presence of the reinforcement particles in the MMC. Short chips were formed under almost all conditions. With the non-reinforced alloy chips of almost similar shape (long and unbroaken) were formed for all cutting conditions.

(v) Particles did not influence shear and friction angles significantly with the variation of feed, i.e., with the increase of feed shear angle increased and friction angle decreased, though the rate of variation depended on feed. For the MMC, shear and friction angles increased very little with the increase of speed. For the non-reinforced alloy initially shear angle decreased and friction angle increased at low speed but after certain speed shear angle increased and friction angle remained constant with further increase of speed.

(vi) The relationship between ϕ and $(\beta - \gamma)$ for the non-reinforced matrix material, i.e., $\phi = B\text{-}C(\beta - \gamma)$, still holds for the MMC. The value of C is $\frac{1}{2}$ for both materials and values of B are $\frac{\pi}{5}$ and $\frac{\pi}{4}$ for the MMC and non-reinforced matrix material, respectively. Chip thickness, and hence shear plane angle, depends on tool rake angle, friction and work hardening. The above relation shows the influence of the reinforcement particles on the variations of shear angle, friction angle and rake angle. With this relationship, cutting forces and contact stresses at the chip-tool interfaces can be estimated more accurately.

Acknowledgements

The authors wish to thank the Australian Research Council for financial assistance. AP is under IPRS and IPA scholarships.

References

[1] R. M. Rashad and T. M. El-Hossainy, "Machinability of 7116 structural aluminum alloy", Materials and Manufacturing Processes, 21: 23–27, 2006.

[2] W. Pedersen, M. Ramulu, "Facing SiCp/Mg metal matrix composites with carbide tools", Journal of Materials Processing Technology 172 (2006) 417–423.

[3] S. Suresh, A. Mortensen, A. Needleman, "Fundamentals of metal matrix composites", Butterworth-Heinemann (1993), Stoneham, MA 02180, USA.

[4] A. Pramanik, L. C. Zhang, J. A. Arsecularatne, "Prediction of cutting forces in machining of metal matrix composites", International Journal of Machine Tools and Manufacture 46(2006) 1795-1803.

[5] Z. F. Zhang, L.C. Zhang, Y. W. Mai, "Wear of ceramic particle-reinforced metal-matrix composites: Part I Wear mechanism", Journal of Material Science 30(1995) 1961-1966.

[6] Z. F. Zhang, L. C. Zhang, and Y.W. Mai, "Particle effects on friction and wear of aluminium matrix composites", Journal of Materials Science, 30(23) (1995) 5999-6004.

[7] C. Yan and L. C. Zhang, "Single-Point Scratching of 6061 Al Alloy reinforced by Different Ceramic Particles", Applied Composite Materials, 1(1995) 431-447.

[8] Z. F. Zhang, L. C. Zhang and Y.W. Mai, "Modeling steady wear of steel/Al_2O_3-Al particle reinforced composite system", Wear, 211(2) (1997) 147-150.

[9] Z. F. Zhang, L. C. Zhang, and Y.W. Mai, “Wear of ceramic particle-reinforced metal-matrix composites, part II a model of adhesive wear”, Journal of Materials Science, 30(8) (1995) 1967-1971.

[10] A. Pramanik, L. C. Zhang, J. A. Arsecularatne, “An FEM investigation into the behaviour of metal matrix composites: tool-particle interaction during orthogonal cutting”, International Journal of Machine Tools & Manufacture 47 (2007) 1497–1506.

[11] A. Pramanik, L. C. Zhang, J. A. Arsecularatne, “Micro-indentation of metal matrix composites -an FEM analysis”, Key Engineering Materials, Vols. 340-341 (2007) pp. 563-570.

[12] A. Pramanik, K.S. Neo, M. Rahman, X.P. Li, M. Sawa, Y. Maeda, “Cutting performance of diamond tools during ultra-precision turning of electroless-nickel plated die materials”, Journal of Materials Processing Technology 140 (2003) 308–313

[13] M. El-Gallab, M. Sklad, “Machining of Al/SiC particulate metal-matrix composites Part I: Tool performance”, Journal of Materials Processing Technology, 83 (1998) 151-158.

[14] X. Ding, W.Y.H. Liew, X.D. Liu, “Evaluation of machining performance of MMC with PCBN and PCD tools”, Wear 259 (2005) 1225-1234.

[15] J. T. Lin, D. Bhattacharyya, C. Lane, “Case study-machinability of a silicon carbide reinforced aluminium metal matrix composite”, Wear, 181-183 (1995) 883-888.

[16] S.S. Joshi, N. Ramakrishnan, P. Ramakrishnan, “Analysis of chip breaking during orthogonal machining of Al/SiCp composites”, Journal of Materials Processing Technology 88 (1999) 90–96.

[17] R. Karthikeyan, G. Ganesan, R.S. Nagarazan, B. C. Pai, “A critical study on machining of Al/SiC composites”, Materials and Manufacturing Processes, 16(1) (2001) 47-60.

[18] G. E. Dieter, “Mechanical Metallurgy”, SI Metric Edition, McGraw-Hill Book Company (UK) Limited, 1988.

[19] A.H. Clausen, T. Borvik, O.S. Hopperstad, A. Benallal, “Flow and fracture characteristics of aluminium alloy AA5083–H116 asfunction of strain rate, temperature and triaxiality”, Materials Science and Engineering A364 (2004) 260–272.

[20] G. L. Wulf, “The high strain rate compression of 7039 Aluminium”, International Journal of Mechanical Sciences, 20(9), 1978, pp. 609-615.

[21] R. Smerd, S. Winkler, C. Salisbury, M. Worswick, D. Lloyd, M. Finn, “High strain rate tensile testing of automotive aluminum alloy sheet”, International Journal of Impact Engineering, 32, 2005, 541–560.

[22] J.P. Davim, “Application of Merchant theory in machining particulate metal matrix composites”, Materials and Design (2006) in press, doi:10.1016/j.matdes.2006.10.015.

[23] P.L.B. Oxley, The mechanics of machining: an analytical approach to assessing machinability, Ellis Horwood, Chichester, 1989.

[24] S.P.F.C. Jaspers, J.H. Dautzenberg, “Material behaviour in metal cutting: strains, strain rates and temperatures in chip formation”, Journal of Material Processing Technology 121 (2002) 123-135.

[25] Y. Li, K.T. Ramesha, E.S.C. Chin, “The mechanical response of an A359/SiCp MMC and the A359 aluminum matrix to dynamic shearing deformations”, Materials Science and Engineering A 382 (2004) 162–170.

[26] Y. Li and K. T. Ramesh, “Influence of particle volume fraction, shape, and aspect ratio on the behavior of particle-reinforced metal matrix composites at high rates of strain”, Acta mater. Vol. 46, No. 16, pp. 5633-5646, 1998.

[27] Y. Li, K.T. Ramesh, E.S.C. Chin, “The compressive viscoplastic response of an A359/SiCp metal-matrix composite and of the A359 aluminum alloy matrix”, International Journal of Solids and Structures 37 (2000) 7547-7562.

[28] D.R. Chichili, K.T. Ramesh, , "Dynamic failure mechanisms in a 6061-T6 Al/Al_2O_3 metal-matrix composite", International Journal of Solids and Structures, v 32, n 17-18, Sept, 1995, p 2609-2626.

[29] S. Yadav, D.R. Chichili, K.T. Ramesh**, "**Mechanical response of a 6061-T6 Al/Al_2O_3 metal matrix composite at high rates of deformation", Acta Metallurgica et Materialia, v 43, n 12, Dec, 1995, p 4453

[30] N.P. Hung, S.H. Yeo, K. K. Lee, K.J. Ng, "Chip formation in machining particulate-reinforced metal matrix composites", Materials and Manufacturing Processes, Vol. 13, No. 1 pp 85-100, 1998.

[31] Y. Ozcatalbas, "Chip and built-up edge formation in the machining of in situ Al_4C_3–Al composite" Materials and Design 24 (2003) 215–221.

[32] M. El-Gallab, M. Sklad, "Machining of Al/SiC particulate metal-matrix composites Part II: Workpiece surface integrity", Journal of materials Processing Technology, 83 (1998) 277-285.

[33] K. Liu, S.N. Melkote, "Effect of plastic side flow on surface roughness in micro-turning process", International Journal of Machine Tools & Manufacture 46 (2006) 1778–1785.

[34] C.B. Lin, Y.W. Hung, Woe-Chun Liu, Shung-Wen Kang, "Machining and fuidity of 356Al/SiC(p) composites", Journal of Materials Processing Technology 110 (2001) 152-159.

[35] E. Capello, "Residual stress in turning Part I: Influence of process parameters" Journal of Materials Processing Technology, 160 (2005) 221-228.

[36] M. H. El-Axir, "A method of modeling residual stress distribution in turning for different materials", International Journal of Machine Tools & Manufacture 42 (2002) 1055–1063.

[37] C. Shet, X. Deng, "Residual stresses and strains in orthogonal metal cutting", International Journal of Machine Tools & Manufacture 43 (2003) 573–587.

[38] S. Mittal. C.R. Liu, "A method of modeling residual stresses in superfinish hard turning", Wear 218 (1998) 21-33.

[39] E. Brinksmeier, J. T. Cammett, W. Koenig, P. Leskovar, J. Peters, H. K. "Residual stresses - measurement and causes in machining processes", CIRP Annals, 31(2), 1982, p 491-510.

[40] I. S. Jawahir, "On the controllability of chip breaking cycles and modes of chip breaking in metal machining" Annals of the CIRP 39(1) (1990) 47-51.

[41] P.L.B Oxley, "Shear angle solutions in orthogonal machining", International Journal of Machine Tool Design and Research, vol. 2 (3), 1962, pp. 219-229.

[42] E. Ng, D. K. Aspinwall, "The effect of workpiece hardness and cutting speed on the machinability of AISI H13 hot work die steel when using PCBN tooling", Transaction of the ASME, Vol. 124, August 2002, 588-594.

[43] H. A. Kishawy, S. Kannan, M. Balazinski, "An energy based analytical force model for orthogonal cutting of metal matrix composites", Annals of the CIRP, vol. 53/1/2004, 91-94.

[44] S. Y. Hong, Y. Ding, R. G. Ekkens, "Improving low carbon steel chip breakability by cryogenic chip cooling", International Journal of Machine Tools & Manufacture 39 (1999) 1065–1085.

[45] J.P. Davim, J. Silva, A.M. Baptista, "Experimental cutting model of metal matrix composites (MMCs), Journal of Materials Processing Technology, 183 (2-3), 2007, p 358-362

[46] M. E. Merchant, "Mechanics of the metal cutting process. I. Orthogonal cutting and type 2 chip", Journal of Applied Physics, (1944) 267-275.

[47] E. H. Lee, B. W. Shaffer, "The theory of plasticity applied to a problem of machining", Journal of Applied Mechanics, December (1951) 15-20.

[48] S. Kobayashi, E. G. Thomsen, "Some observations on shearing process in metal cutting", Transactions of the ASME, Journal of Engineering for Industry, August (1959) 251-261.

[49] H.L.D. Pugh, "Mechanics of cutting process", Proceedings, Conference on Technology of Engineering Manufacture, The Institute of Mechanical Engineers, (1958) 237-254.

Captions for figures

Fig. 1. Experimental parameters and setup: (1) chuck to hold work piece, (2) workpiece in bar shape, (3) cutting tool insert, (4) tool holder, and (5) piezo-electric dynamometer.

Fig. 2. Variation of forces with feed (at speed 400 m/min, depth of cut 1 mm): (a) cutting forces; (b) thrust forces

Fig. 3. Variation of forces with speed (at feed 0.1 mm/rev, depth of cut 1 mm): (a) cutting forces; (b) thrust forces

Fig. 4. Effect of feed on the percentages of different force components in (a) cutting (b) thrust directions (at speed 400 m/min, depth of cut 1 mm)

Fig. 5. Effect of speed on the percentages of different force components in (a) cutting (b) thrust directions (at feed 0.1mm/rev, depth of cut 1 mm)

Fig. 6. Variation of shear strength with (at depth of cut 1 mm): (a) feed (at speed 400 m/min); (b) speed (at feed 0.1 mm/rev)

Fig. 7. Force signals at different cutting conditions during machining of MMC and non-reinforced alloy (at depth of cut 1 mm): (a) feed 0.025 mm/rev and speed 400 m/min; (b) feed 0.4 mm/rev and speed 400 m/min; (c) Speed 100 m/min and feed 0.1 mm/rev; (d) Speed 800 m/min and feed 0.1 mm/rev

Fig. 8. Effect of feed on surface roughness (at speed 400 m/min, depth of cut 1 mm): (a) R_a; (b) R_{max}

Fig. 9. Machined surface of the MMC at different feeds (at speed 400 m/min, depth of cut 1 mm)

Fig. 10. Machined surface of the non-reinforced alloy at different feeds (at speed 400 m/min, depth of cut 1 mm)

Fig. 11. Effect of speed on surface roughness (at feed 0.1 mm/rev, depth of cut 1 mm): (a) R_a; (b) R_{max}

Fig. 12. Machined surface of the MMC at different speeds (at feed 0.1 mm/rev, depth of cut 1 mm)

Fig. 13. Machined surface of the non-reinforced alloy at different speeds (at feed 0.1 mm/rev, depth of cut 1 mm)

Input parameters
Feed
Cutting speed
Workpiece composition

Output parameters
Force
Surface roughness
Residual stress
Chip shape
Shear and friction angles

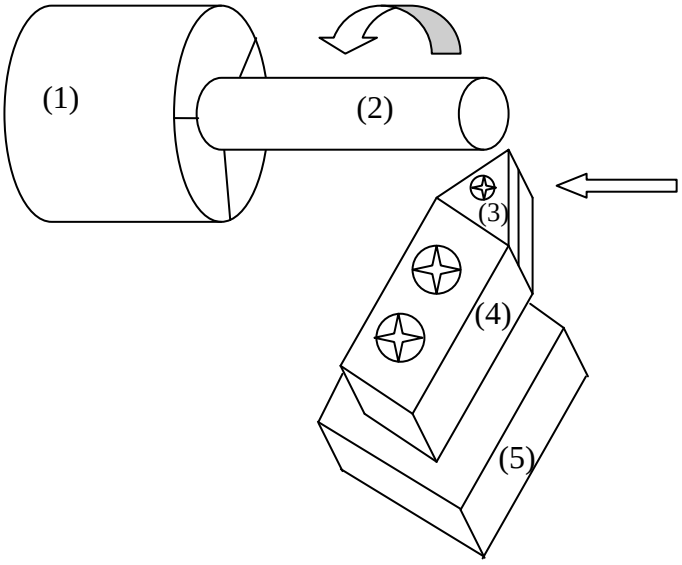

Fig. 1. Experimental parameters and setup: (1) chuck to hold work piece, (2) workpiece in bar shape, (3) cutting tool insert, (4) tool holder, and (5) piezo-electric dynamometer.

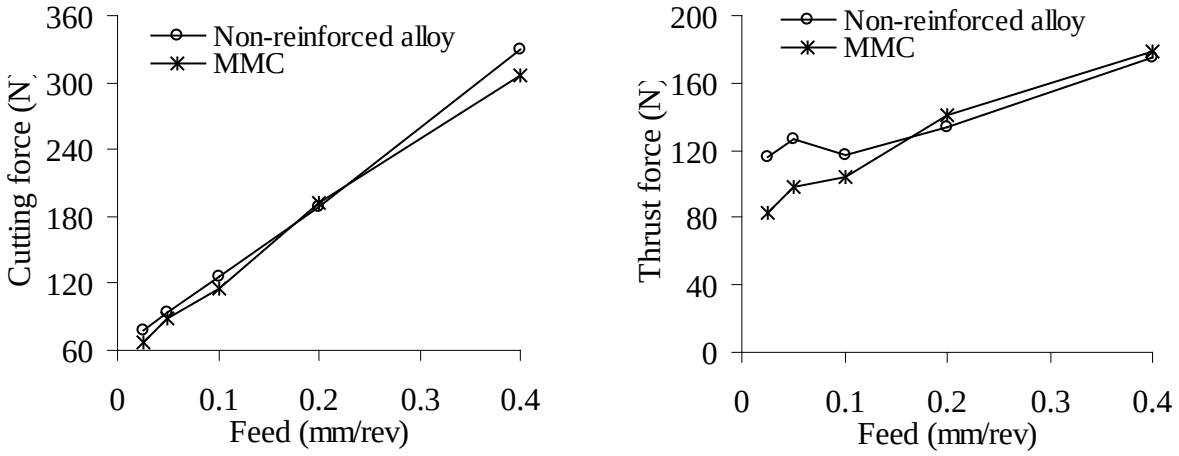

(a) (b)

Fig. 2. Variation of forces with feed (at speed 400 m/min, depth of cut 1 mm): (a) cutting forces; (b) thrust forces

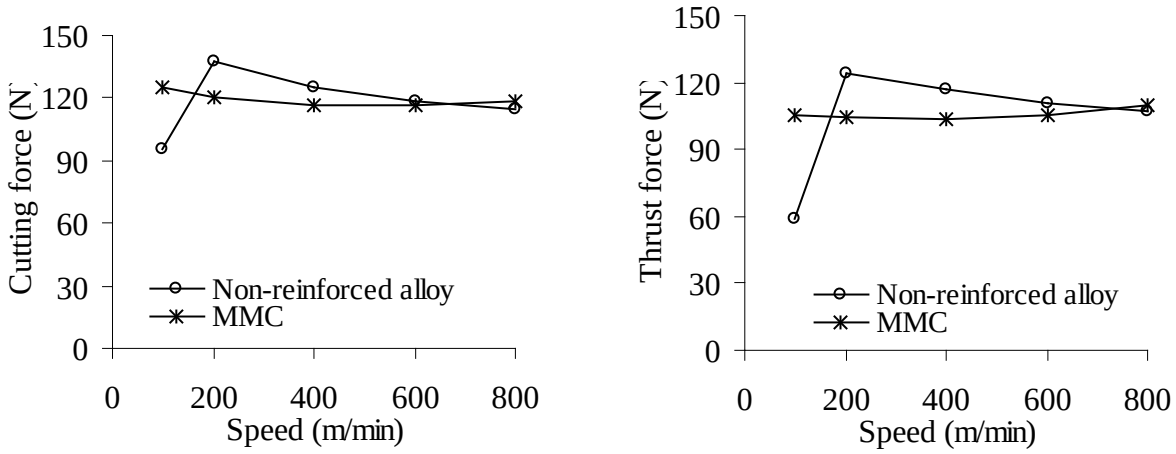

(a) (b)

Fig. 3. Variation of forces with speed (at feed 0.1 mm/rev, depth of cut 1 mm): (a) cutting forces; (b) thrust forces

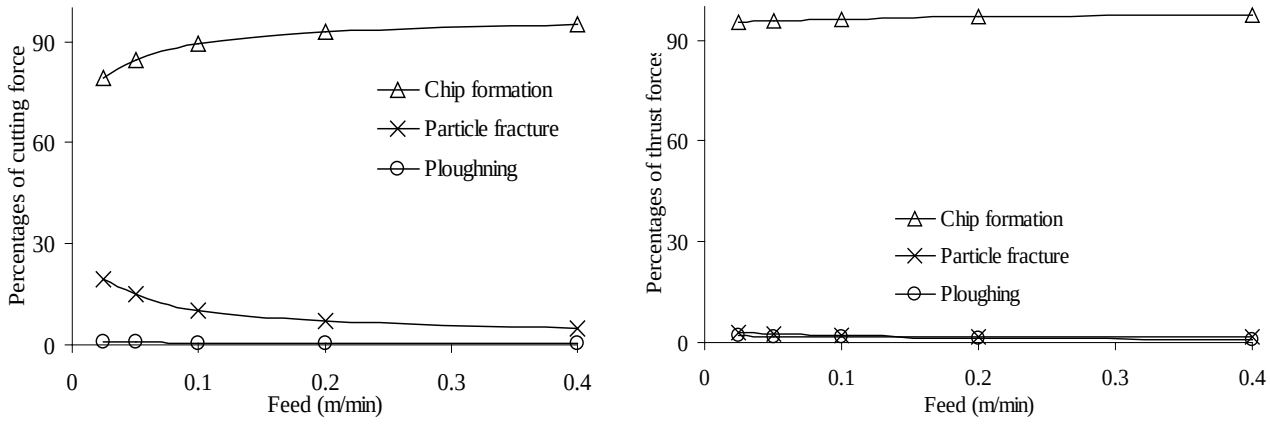

(a) (b)

Fig. 4. Effect of feed on the percentages of different force components in (a) cutting (b) thrust directions (at speed 400 m/min, depth of cut 1 mm)

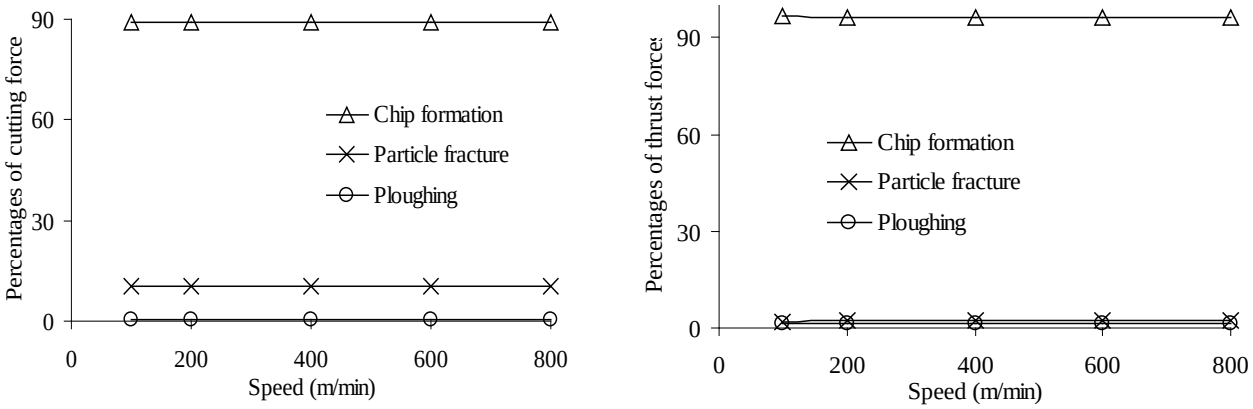

(a) (b)

Fig. 5. Effect of speed on the percentages of different force components in (a) cutting (b) thrust directions (at feed 0.1 mm/rev, depth of cut 1 mm)

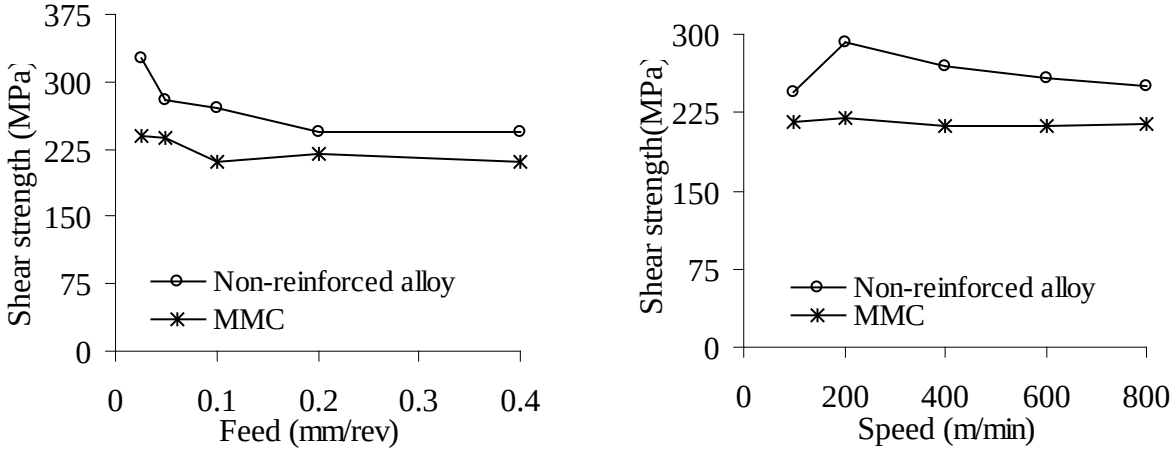

(a) (b)

Fig. 6. Variation of shear strength with (at depth of cut 1 mm): (a) feed (at speed 400 m/min); (b) speed (at feed 0.1 mm/rev)

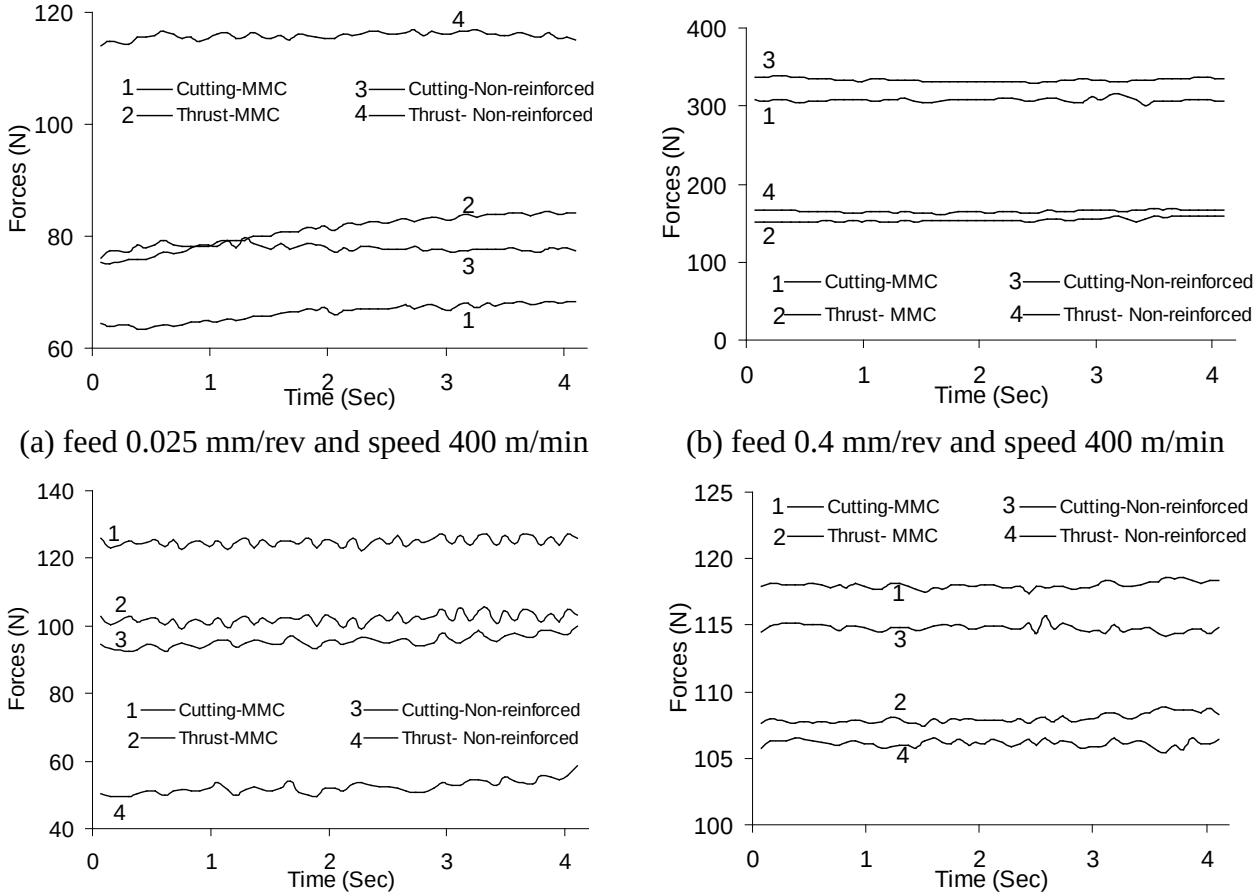

(a) feed 0.025 mm/rev and speed 400 m/min

(b) feed 0.4 mm/rev and speed 400 m/min

(c) Speed 100 m/min and feed 0.1 mm/rev

(d) Speed 800 m/min and feed 0.1 mm/rev

Fig. 7. Force signals at different cutting conditions during machining of MMC and non-reinforced alloy (at depth of cut 1 mm)

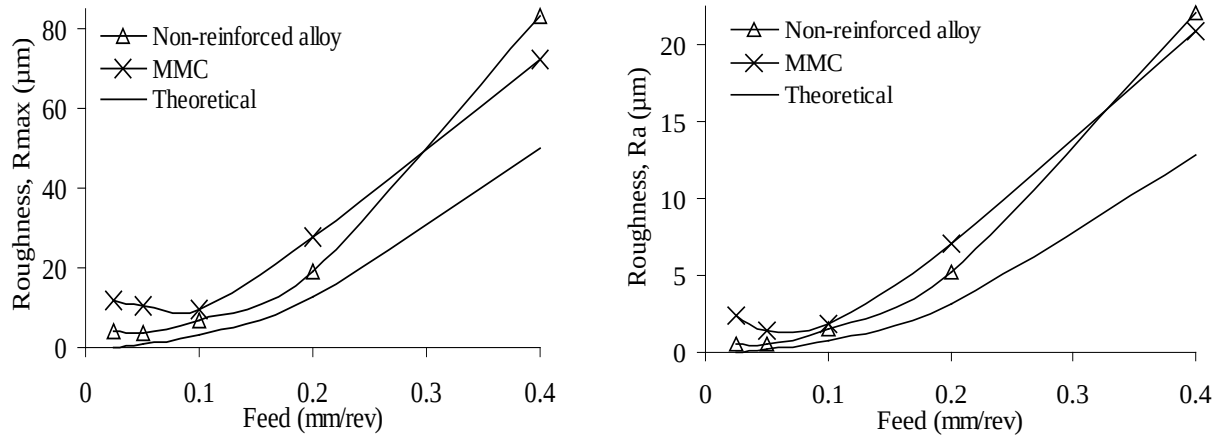

(a) (b)

Fig. 8. Effect of feed on surface roughness (at speed 400 m/min, depth of cut 1 mm): (a) R_a; (b) R_{max}

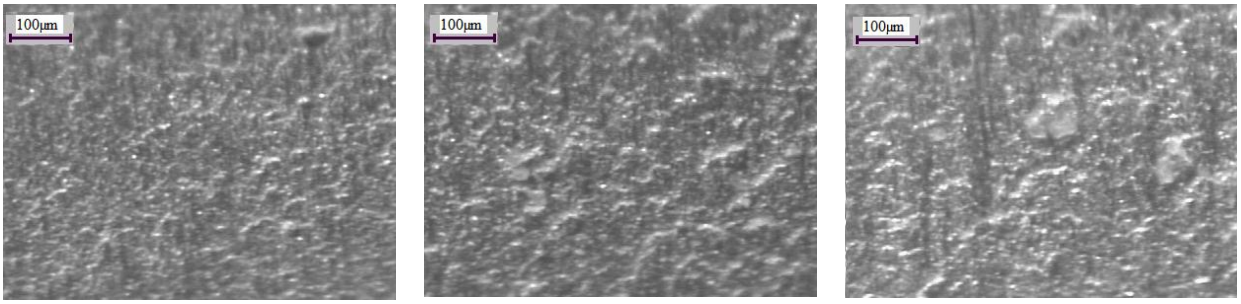

0.025 mm/rev 0.05 mm/rev 0.1 mm/rev

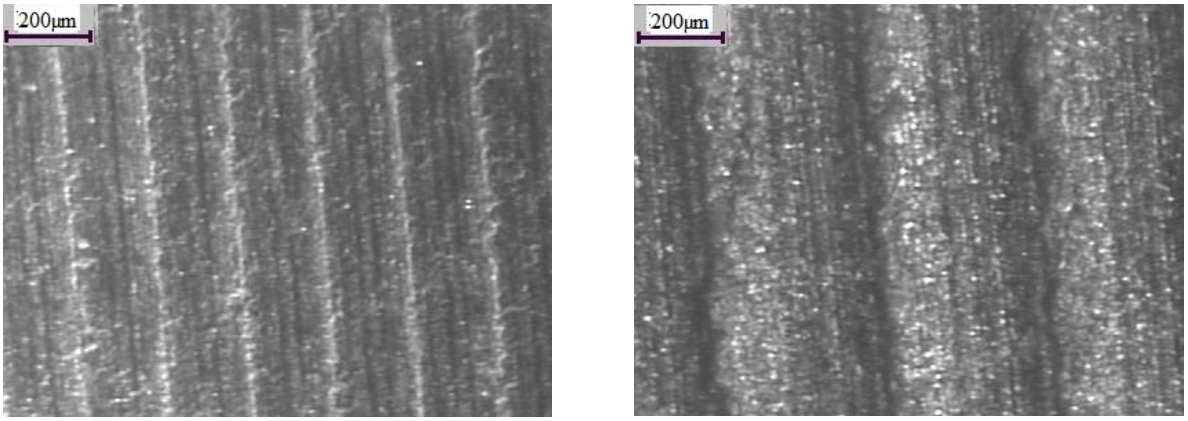

0.2 mm/rev 0.4 mm/rev

Fig. 9. Machined surface of the MMC at different feeds (at speed 400 m/min, depth of cut 1 mm)

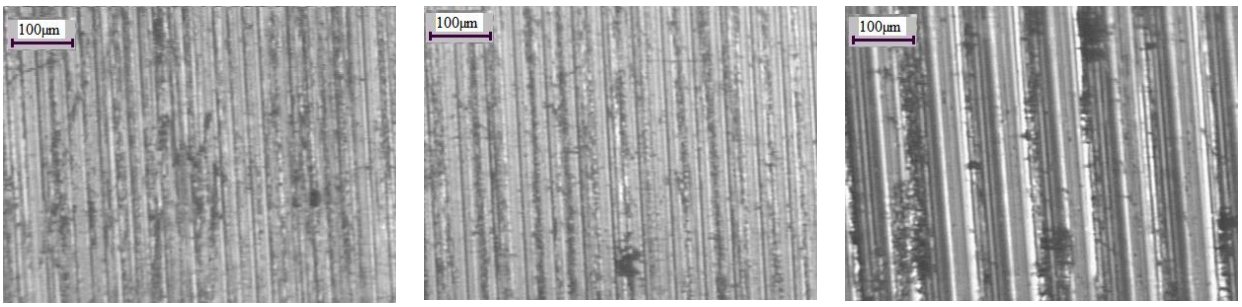

0.025 mm/rev 0.05 mm/rev 0.1 mm/rev

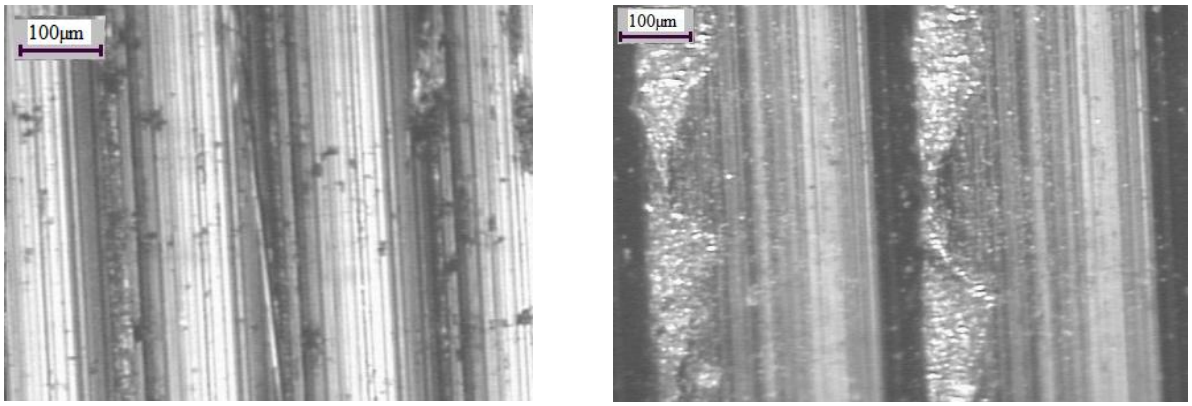

0.2 mm/rev 0.4 mm/rev

Fig. 10. Machined surface of non-reinforced alloy at different feeds (at speed 400 m/min, depth of cut 1 mm)

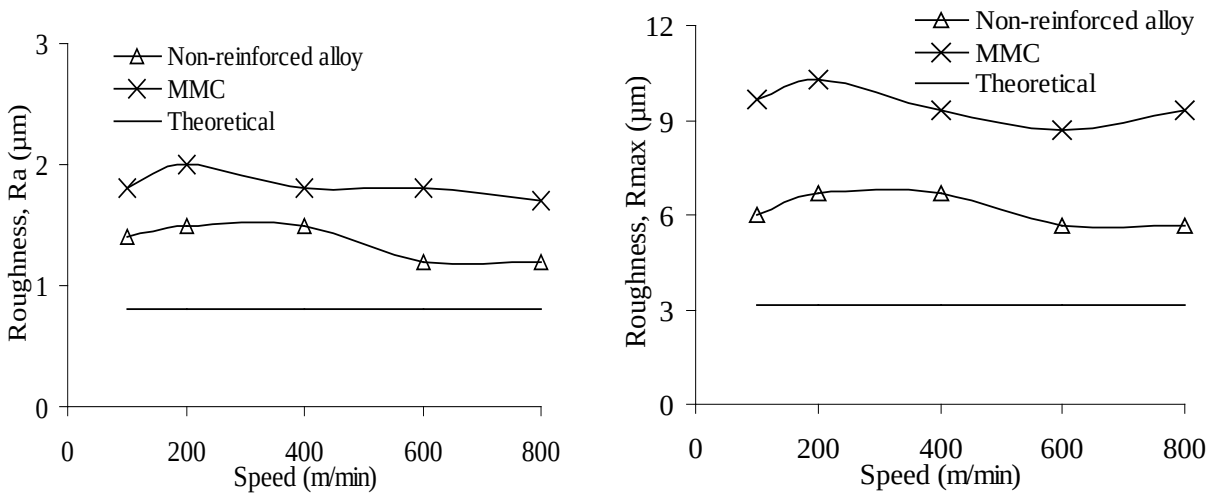

(a) (b)

Fig. 11. Effect of speed on surface roughness (at feed 0.1 mm/rev, depth of cut 1 mm): (a) R_a; (b) R_{max}

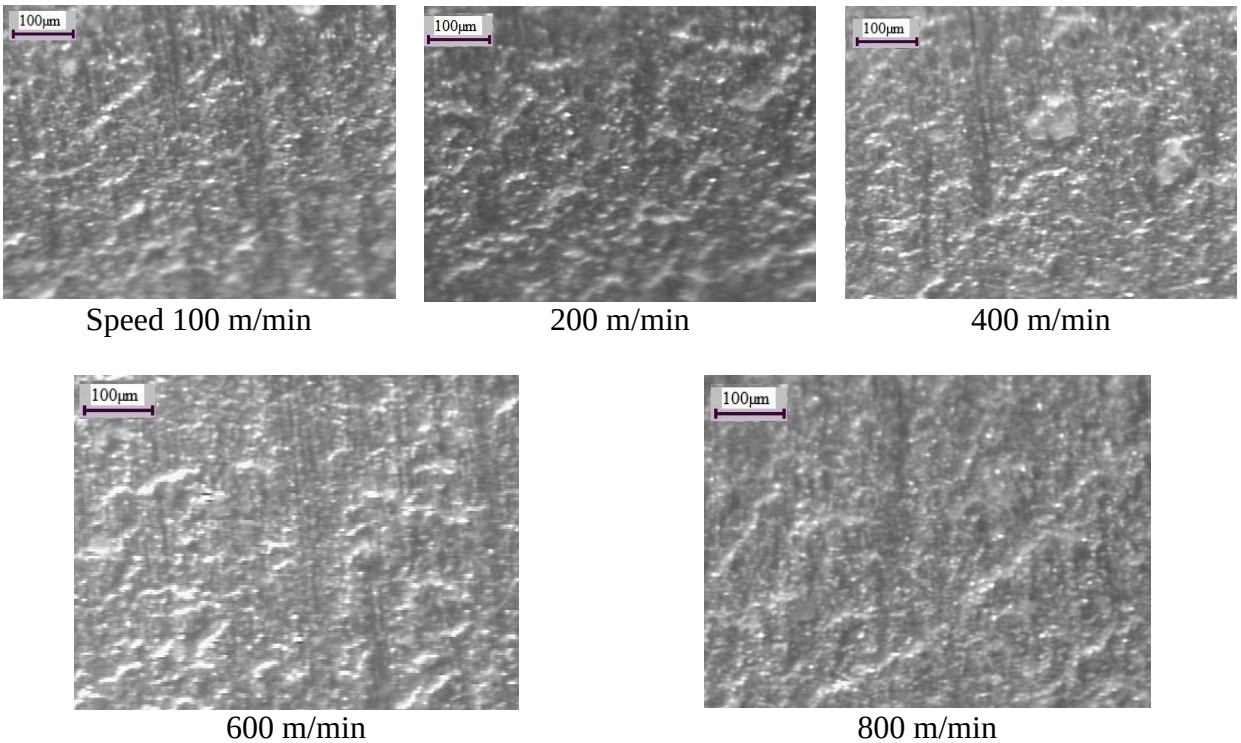

Speed 100 m/min 200 m/min 400 m/min

600 m/min 800 m/min

Fig. 12. Machined surface of the MMC at different speeds (at feed 0.1 mm/rev, depth of cut 1 mm)

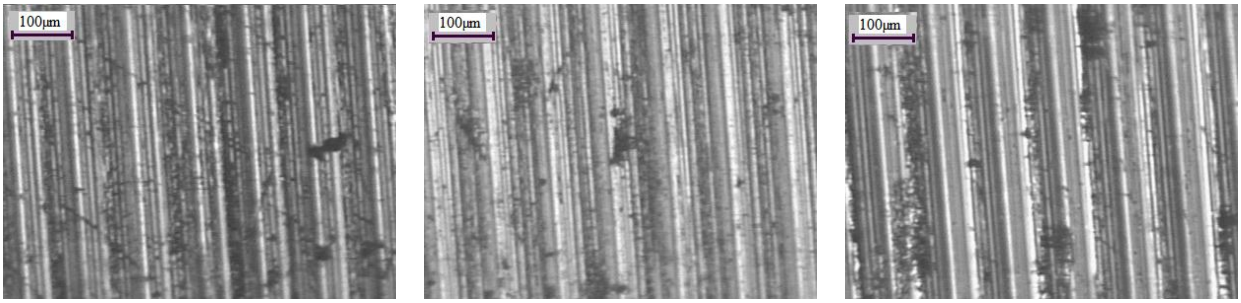

Speed 100 m/min 200 m/min 400 m/min

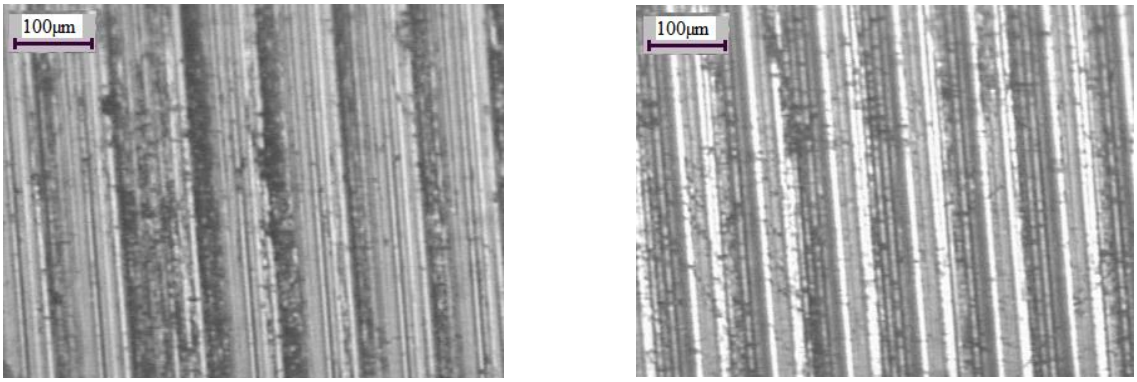

600 m/min 800 m/min

Fig. 13. Machined surface of the non-reinforced alloy at different speeds (at feed 0.1 mm/rev, depth of cut 1 mm)

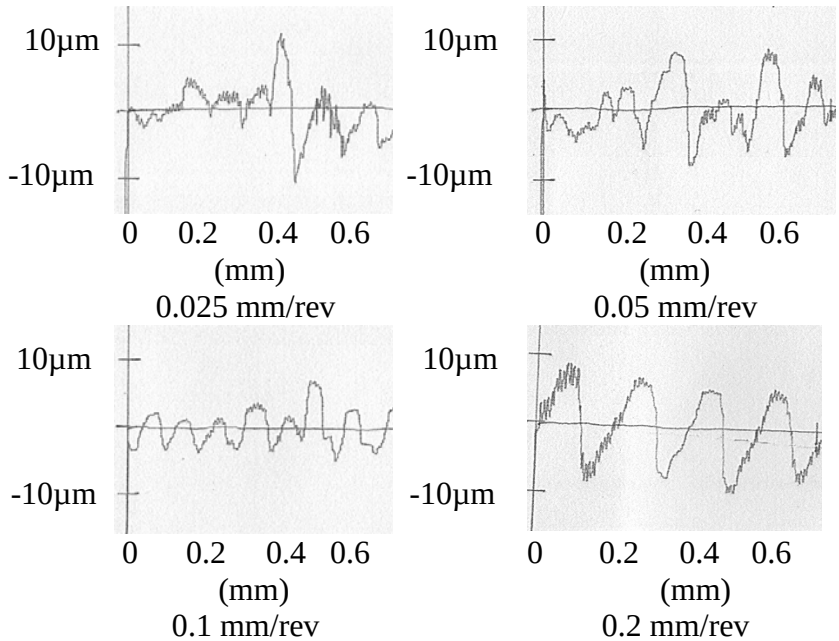

Fig. 14. Machined surface profile of the MMC at different feeds

(at speed 400 m/min, depth of cut 1 mm)

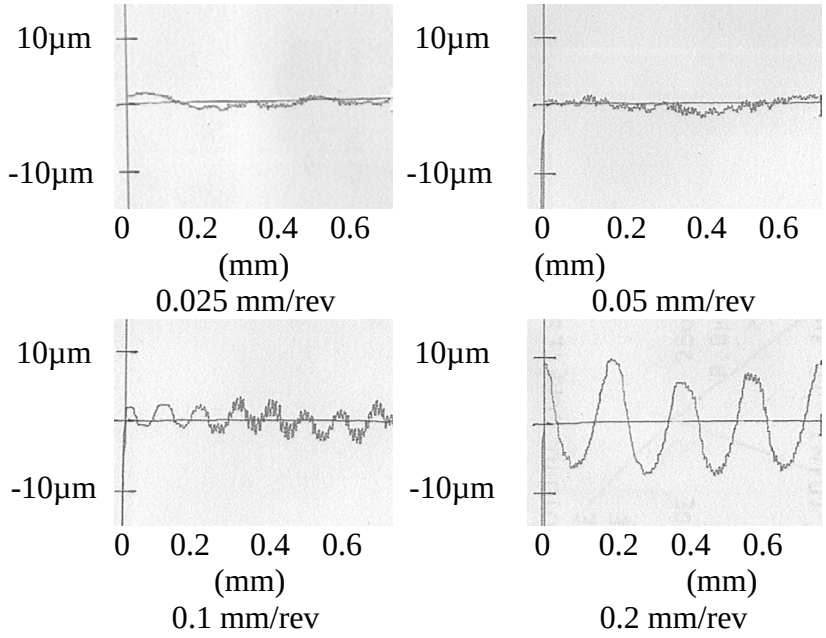

Fig. 15. Machined surface profile of the non-reinforced alloy at different feeds (at speed 400 m/min, depth of cut 1 mm)

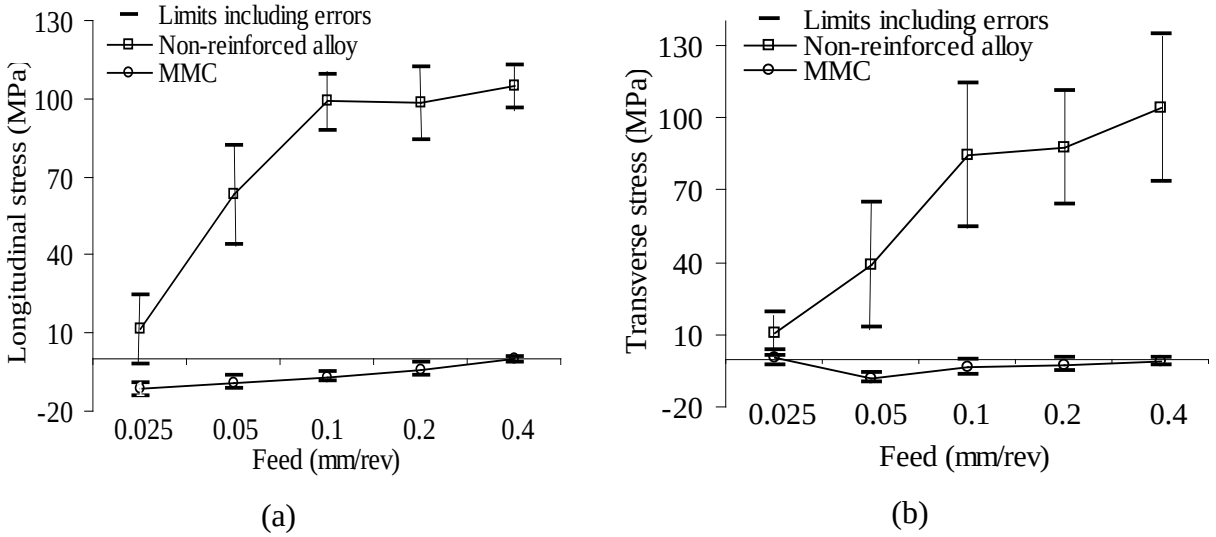

Fig. 16. Effect of feed on residual stress (at speed 400 m/min, depth of cut 1 mm): (a) longitudinal; (b) transverse

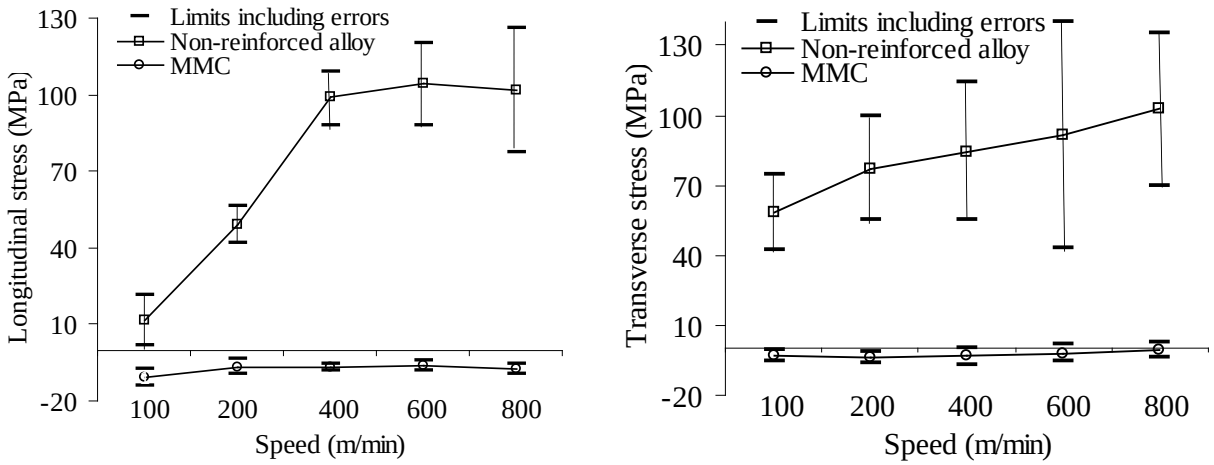

(a) (b)

Fig. 17. Effect of speed on residual stress (at feed 0.1 mm/rev, depth of cut 1 mm): (a) longitudinal; (b) transverse

0.025 mm/rev 0.05 mm/rev 0.1 mm/rev

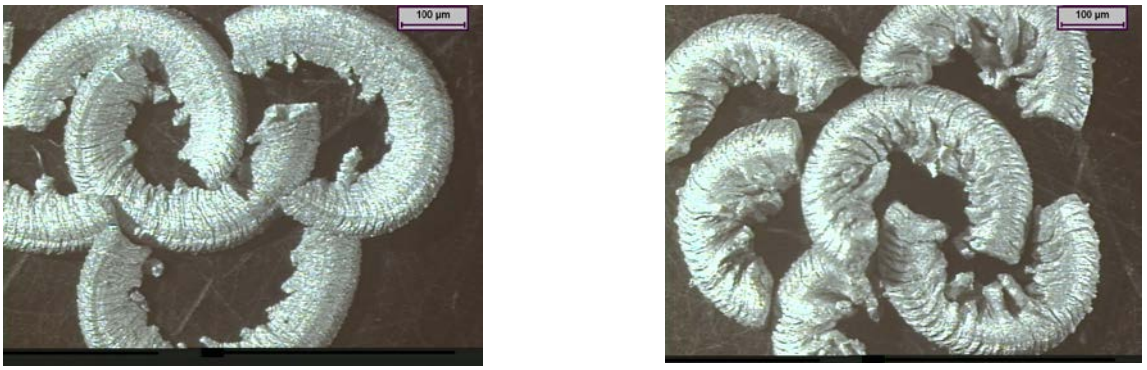

0.2 mm/rev 0.4 mm/rev

Fig. 18. Chip shapes of the MMC at different feeds (at speed 400 m/min, depth of cut 1 mm)

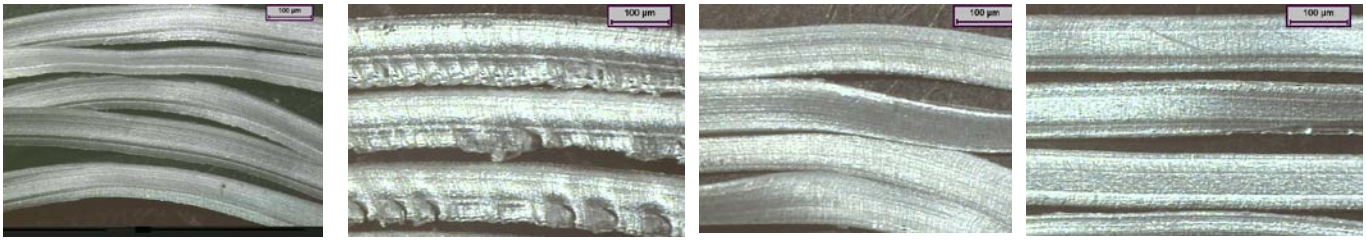

Feed 0.025 mm/rev speed 400 m/min | Feed 0.4 mm/rev speed 400 m/min | Speed 200 m/min feed 0.1 mm/rev | Speed 800 m/min feed 0.1 mm/rev

Fig. 19. Chip shapes of non-reinforced alloy at different cutting conditions (at depth of cut 1 mm)

Speed 100 m/min | 200 m/min | 400 m/min

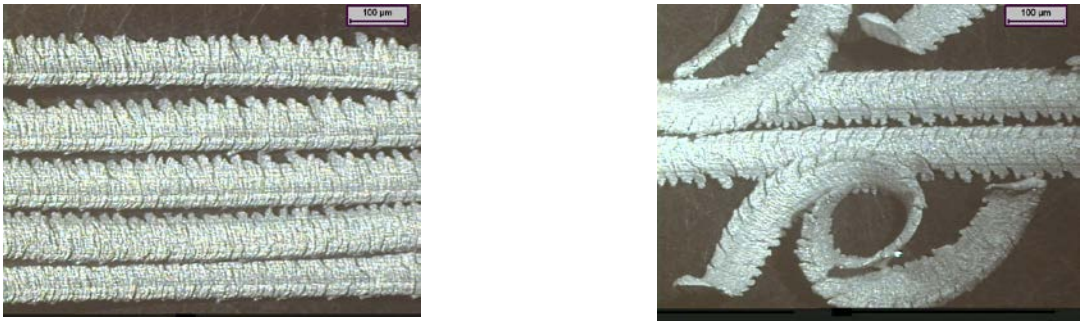

600 m/min | 800 m/min

Fig. 20. Chip shapes of the MMC at different speeds (at feed 0.1 mm/rev, depth of cut 1 mm)

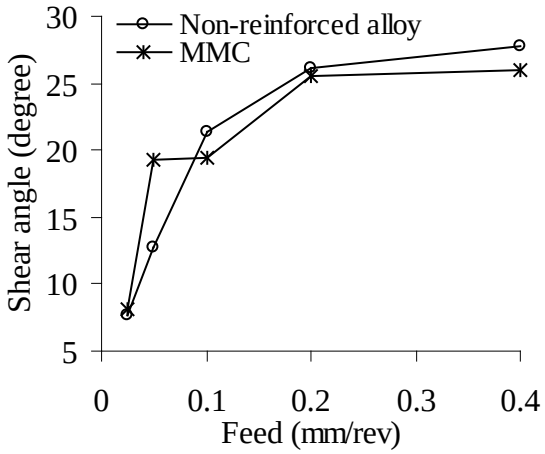

(a)

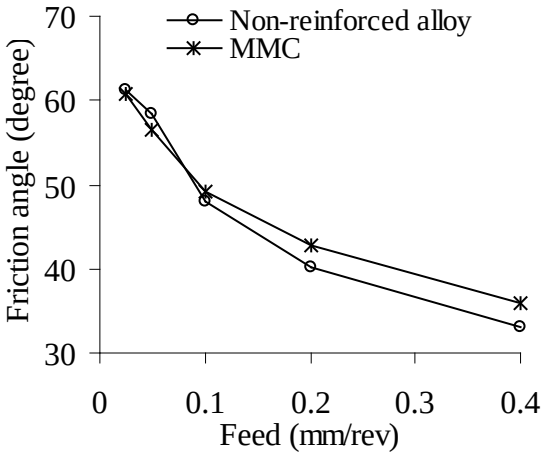

(b)

Fig. 21. Effect of feed on shear and friction angles (at speed 400 m/min, depth of cut 1 mm): (a) shear angle; (b) friction angle

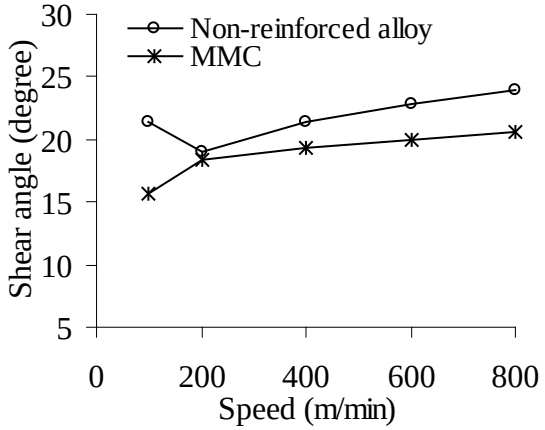

(a)

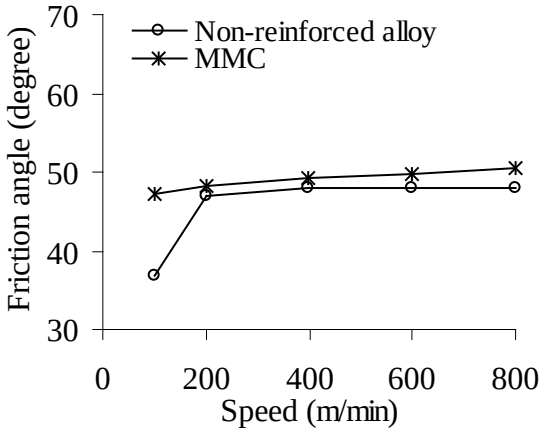

(b)

Fig. 22. Effect of speed on shear and friction angles (at feed 0.1 mm/rev, depth of cut 1 mm): (a) shear angle; (b) friction angle

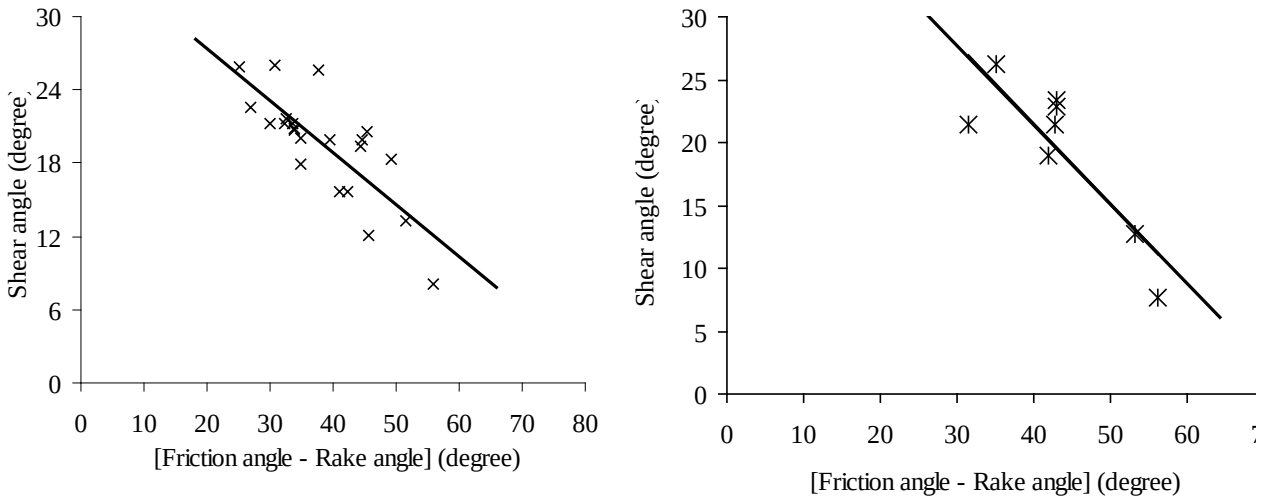

(a) (b)

Fig. 23. Shear angle, ϕ versus [Friction angle, β – Rake angle, γ] relationship: (a) for the MMC; (b) for the non-reinforced alloy